Skin effect in steel sheets under rotating induction

C Appino, O Hamrit, F Fiorillo, C Ragusa, Olivier de La Barrière, F Mazaleyrat, M Lobue

Skin effect in steel sheets under rotating induction

C. Appino[1], O. Hamrit[2], F. Fiorillo[1], C. Ragusa[3], O. de la Barrière[2a], F. Mazaleyrat[2], M. LoBue[2]

[1]Istituto Nazionale di Ricerca Metrologica (INRIM), Strada delle cacce 91, 10135 Torino, Italy
[2]SATIE, ENS Cachan, CNRS, UniverSud, 61 av. du Président Wilson, F-94230 Cachan, France
[3]Dipartamento Energia, Politecnico di Torino, C.so Duca degli Abruzzi 24, 10129 Torino, Italy

[a] Corresponding author. Electronic address: barriere@satie.ens-cachan.fr, telephone and fax: 0033147402125. Address: 61 avenue du Président Wilson, F-94230 Cachan, France.

Abstract

By means of a newly developed broadband measuring setup we have overcome the usual upper limit for the test frequency, around a few hundred Hz, which is encountered in the two-dimensional characterization of magnetic steel sheets at technical inductions and we have measured the rotational losses in low-carbon steels up to 1 kHz and peak induction 1.7 T. An important piece of information is thus retrieved upon a frequency range useful to predict the performance of high-speed electrical machines. Our experiments, performed on thick (0.640 mm) laminations, have brought to light the emergence of the skin effect under rotational fields. This is revealed by an abrupt deviation of the excess loss component, calculated under the conventional loss separation procedure, from its well-known linear dependence on the square root of the frequency. A simple magnetic constitutive law under rotating induction is proposed and introduced into the electromagnetic diffusion equation, which is solved by finite elements coupled to a non-linear algorithm. The classical rotational eddy current loss, largely prevalent with respect to the hysteresis and excess loss components on approaching the kHz frequencies in low-carbon steels, is then calculated in the presence of skin effect, permitting one to achieve full analysis of the rotational losses and good predicting capability upon a broad range of frequencies and peak inductions.

Keywords

Magnetic losses, circular induction, non-oriented magnetic steel, skin effect.

1- Introduction

In electrical traction applications, compact geometry and maximum torque density of motors are obtained by increasing the rotating speed [1, 2], with ensuing high conversion frequencies, greater iron losses, and decreasing efficiency. A compromise must then be found at the design stage between these competing issues, a reason for requiring accurate broadband magnetic loss characterization of the laminations used in the machine cores and a relatively simple implementation of loss modeling. The loss decomposition procedure, including the case of distorted induction, is the standard modeling response to the loss phenomenology at low-to-medium frequencies, where the skin effect can be neglected [3, 4]. Starting from solid physical analysis, it provides a simple three-term expression for the measured energy loss $W(f) = W_{hyst} + W_{class}(f) + W_{exc}(f)$, where the quasi-static term W_{hyst} combines with a dynamic contribution $W_{dyn}(f) = W_{class}(f) + W_{exc}(f)$, the sum of the classical and the excess components, which depend on the magnetizing frequency like f and $f^{1/2}$, respectively [3]. When, under increasing f, eddy current shielding gives rise to skin depth comparable to or lower than the lamination half-thickness, straightforward loss separation cannot be accomplished and the calculation of the dynamic loss component via the electromagnetic diffusion equation requires modeling (for example, via the Preisach model of hysteresis) of the constitutive equation of the material and the use of numerical methods [5-8].

Experimental results have shown that conventional loss separation can be applied, in the absence of skin effect, to the two-dimensional losses, and one can express, in particular, the rotational losses as $W^{(ROT)}(f) = W_{hyst}^{(ROT)} + W_{class}^{(ROT)}(f) + W_{exc}^{(ROT)}(f)$, with the same $W_{class}^{(ROT)} \propto f$ and $W_{exc}^{(ROT)} \propto f^{1/2}$ dependences found under alternating fields [9]. Very little is known, however, on the behavior of the rotational losses beyond a few hundred Hz [10], that is, under the regimes pertaining to high-speed electrical machines, where skin effect will expectedly take place.

We have employed a recently developed 2D setup, based on a three-phase magnetizer [11], to attain rotational induction levels of technical interest (e.g. J_p = 1.5 T and beyond) in non-oriented steel sheets up to the kHz range [12]. We have investigated, in particular, the rotational loss behavior versus frequency of low-carbon steel sheets, 0.640 mm thick, up to 1 kHz and peak polarization J_p = 1.7 T. Conductivity and thickness of these sheets are sufficient to generate a surge of the skin effect already at power frequencies. A sort of frequency threshold for it is in fact identified, where an attendant sharp deviation of $W_{exc}^{(ROT)}$ from the usual $f^{1/2}$ dependence is put in evidence when applying the standard loss decomposition procedure. This appears to be a unique simple experimental route to direct recognition of growing skin effect. It also highlights the conceptually important role of the excess component in the loss analysis, even if, as in the present case, it marginal contributes to the total loss figure. To calculate the classical loss, by far the largest component in the upper frequency range, it is recognized that, thanks to the near-isotropic properties of the material, the magnetic constitutive law $B(H)$ under rotational field can be well approximated, along any of two orthogonal directions, by a simple relationship between complex quantities of the type $\underline{B} = \underline{\mu}(|\underline{H}|) \cdot \underline{H}$. This permits one to solve the electromagnetic diffusion equation by conventional numerical technique and to calculate $W_{class}^{(ROT)}(f)$, eventually attaining good prediction of $W^{(ROT)}(f)$ upon the whole investigated frequency range.

2. Experimental results: evidence for the skin effect

A three-phase magnetizer, especially designed to reach high frequencies [11], has been employed in the measurement of the magnetic losses in low-carbon steel sheets (density δ = 7850 kg/m^3, thickness d = 0.640 mm, resistivity $\rho = 12.51 \cdot 10^{-8}$ Ω·m) under digitally controlled circular flux loci [13]. The magnetic losses have been measured by the fieldmetric method [14-15] on 80 mm diameter circular samples, accurately centred in the stator-like magnetizer. A small air-gap of 1 mm permits one to minimize the required exciting power, which is supplied by triple DC-20 kHz 5 kVA power amplifier (CROWN 5000VZ). The orthogonal B and H windings are placed on a 20 mm × 20 mm measuring area at the centre of the disk. The measurements are repeated, for any polarization and frequency value, under clockwise and counterclockwise rotation and their average is taken as the resulting loss figure $W^{(ROT)}(J_p, f)$. Fig. 1 shows the experimental dependence of the measured rotational loss on J_p (negligibly different everywhere from the peak induction B_p) up to 1.7 T for frequencies ranging between 2 Hz and 1kHz. It is noted how the maximum of $W^{(ROT)}(f)$ versus J_p, occurring around J_p = 1.5 T, tends to disappear beyond about 50 Hz, because of the growing influence of the monotonically increasing classical loss component. It is also remarked that the upper values of the here attained product $J_p \cdot f$ (e.g., J_p = 1.5 T at f = 1 kHz) are significantly larger than present literature limits [10].

According to the standard analysis performed at power frequencies in nonoriented Fe-Si laminations [9], the rotational hysteresis $W_{hyst}^{(ROT)}$ is found by extrapolating $W^{(ROT)}(J_p, f)$ to f = 0 and we calculate the classical loss $W_{class}^{(ROT)}(f)$ as

$$W_{class}^{(ROT)}(B_p, f) = \frac{\pi^2}{3} \cdot \frac{d^2 B_p^2}{\rho} f \ . \qquad [\mathrm{J/m^3}] \qquad (1)$$

By making the difference $W_{diff}^{(ROT)}(f) = W^{(ROT)}(f) - W_{class}^{(ROT)}(f) = W_{hyst}^{(ROT)} + W_{exc}^{(ROT)}(f)$, we obtain the behaviors shown in Fig. 2a (symbols), where the quantity $W_{diff}^{(ROT)}(f)$ is plotted against $f^{1/2}$ for three different induction levels. $W_{diff}^{(ROT)}(f)$ strongly deviates, beyond a threshold frequency value f_{thr}, from the usual $f^{1/2}$ dependence (the straight lines in Fig. 2a) experimentally observed below and around power frequencies in 3 wt% Fe-Si laminations [16]. $W_{diff}^{(ROT)}(f)$ follows opposite outward trends with respect to the $f^{1/2}$ straight line below and above $J_p \sim 1$ T, because $W_{class}^{(ROT)}(f)$ tends either to lower or faster than linear dependence on f and Eq. (1) no more applies. Such behavior of $W_{class}^{(ROT)}(f)$ replicates the phenomenology of the alternating classical loss in the presence of the skin effect [3-5] and is further put in evidence by the statistical analysis of the magnetic objects (MO), as defined in Bertotti's theory [3]. Fig. 2 shows the dramatic departure of the number $n(H_{exc})$ of active MOs from the linear increase with $H_{exc} = W_{exc}^{(ROT)}/4J_p$ predicted using Eq. (1). The sharp turnaround of $n(H_{exc})$ occurs exactly at the frequency f_{thr}. The statistical loss analysis provides then us with a direct and unique method to detect the surge of the skin effect in magnetic sheets, even though, like in the present case, $W_{exc}^{(ROT)}$ contributes by a small proportion to $W^{(ROT)}$. We have for example, at J_p = 1.2 T and f_{thr} = 100 Hz, the total rotational loss $W^{(ROT)}$ = 360.5 mJ/kg, composed of $W_{hyst}^{(ROT)}$ = 139.5 mJ/kg, $W_{class}^{(ROT)}$ = 197.5 mJ/kg, and $W_{exc}^{(ROT)}$ = 23.5 mJ/kg. It is remarked that, given the mechanism of the magnetization rotation in nonoriented

materials, there is no room for classical loss formulations deriving from the saturation wave model, as sometimes proposed in the literature [17].

Having thus experimentally identified a threshold frequency for the skin effect, we essentially need to proceed towards a novel formulation for $W_{class}^{(ROT)}(f)$, by which we can cover the rotational loss properties upon the whole broad frequency range.

3. Skin effect and classical eddy current losses under circular induction

3.1 *A simplified constitutive equation*

Some works exist for extending the conventional Preisach models under alternating fields to rotating inductions [18-19]. However, such models are quite heavy from the computational point of view, and do not permit to take into account the decrease of the hysteresis loss when the induction increases under rotating field. To correct these drawbacks, we propose here a simple hysteresis model based on the assimilation of the material to a perfect isotropic medium. Let us take the sheet sample midplane as the *xy*-plane and assume the coordinate $z = 0$ at the center of the disk sample. The magnetization vector is assumed to rotate at constant angular velocity $\omega = 2\pi f$. We need to define a constitutive equation for the material under rotating field, paralleling the usual case of alternating field, where such equation coincides with the static hysteresis loop and a hysteresis model must be worked out [4, 20]. Remarkably, a simple magnetic constitutive law can be adopted with circular polarization in nonoriented alloys, under the following assumptions: 1) The constitutive relationship is rate independent. This amounts to assume, according to the experiments, that in the range of frequencies of interest (i.e., beyond f_{thr}) the excess loss figure $W_{exc}^{(ROT)}$ is much smaller than $W_{hyst}^{(ROT)}$ and $W_{class}^{(ROT)}$; 2) The material anisotropy can be neglected. We approximate here this condition by substituting, at each frequency, the experimental magnetic field locus $\boldsymbol{H}(f)$ associated with the circular $\boldsymbol{B}$-locus (of modulus $B_p = |\boldsymbol{B}|$) with an equivalent circular $\boldsymbol{H}$-locus of same area and radius $H(f)=|\boldsymbol{H}(f)|$, emulating the condition of a perfectly isotropic material. By extrapolating this procedure to $f = 0$, the limiting circle of radius $H_0 = |\boldsymbol{H}_0|$ is obtained, with $\boldsymbol{B}$ lagging behind $\boldsymbol{H}_0$ by the angle θ_{hyst} (see Fig. 3). Under the isotropic approximation, the sinusoidal $\boldsymbol{H}$ and $\boldsymbol{B}$ components are identical along the *x* and *y* axes and the energy loss

$$W^{(ROT)}(B_p, f) = \oint \boldsymbol{H} \cdot \mathrm{d}\boldsymbol{B} = \int_0^{1/f} (H_x \cdot dB_x/dt + H_y \cdot dB_y/dt) = W_x + W_y = 2W_x \ , \qquad [\mathrm{J/m^3}] \quad (2)$$

can be written in the quasi-static limit as $W_{hyst}^{(ROT} = 2\pi H_0 B_p \cdot \sin(\theta_{hyst})$. The phase shift is then obtained as

$$\theta_{hyst}(H_0) = \arcsin\left[\frac{W_{hyst}^{(ROT)}(B_p)}{2\pi H_0 B_p}\right]. \quad (3)$$

At the same time, the complex permeability, embodying the constitutive equation for the material under rotational field, is given by

$$\underline{\mu}(H_0) = \mu(H_0)\exp[-i\theta_{hyst}(H_0)] \quad (4)$$

(with $i^2 = -1$), where $\mu(H_0) = |\underline{\mu}(H_0)| = B_p/H_0$. Both $\underline{\mu}(H_0)$ and θ_{hyst} are time-independent and evolve with the

polarization level in the investigated material as shown in Fig. 4. The complex constitutive equations for the *x* and *y* directions can thus be expressed as $\underline{B}_x = \underline{\mu}(H_x)\underline{H}_x$ and $\underline{B}_y = \underline{\mu}(H_y)\underline{H}_y$, with $H_x = \left|\underline{H}_x\right|$ and $H_y = \left|\underline{H}_y\right|$.

3.2 *Diffusion equation and classical loss*

The electromagnetic diffusion equation, controlling the magnetic field penetration in the sheet, is written, under the usual assumption of infinitely extended *xy*-plane,

$$\frac{\partial^2 \underline{H}_x(z)}{\partial z^2} = i\omega\sigma \underline{B}_x(z) \qquad \frac{\partial^2 \underline{H}_y(z)}{\partial z^2} = i\omega\sigma \underline{B}_y(z) \tag{5}$$

where all the local quantities depend only on *z.* Introducing the constitutive equations in Eq. (5) we get

$$\frac{\partial^2 \underline{H}_x(z)}{\partial z^2} = i\omega\sigma \underline{\mu}(H_x)\underline{H}_x \qquad \frac{\partial^2 \underline{H}_y(z)}{\partial z^2} = i\omega\sigma \underline{\mu}(H_y)\underline{H}_y, \tag{6}$$

to be solved under the boundary conditions

$$\left.\frac{\partial \underline{H}_x(z)}{\partial z}\right|_{z=0} = 0 \qquad \left.\frac{\partial \underline{H}_y(z)}{\partial z}\right|_{z=0} = 0 \tag{7}$$

$$\left.\frac{\partial \underline{H}_x(z)}{\partial z}\right|_{z=d/2} = i\omega\sigma\frac{d}{2}B_p \qquad \left.\frac{\partial \underline{H}_y(z)}{\partial z}\right|_{z=d/2} = i\omega\sigma\frac{d}{2}\left(-iB_p\right) \tag{8}$$

imposed by the symmetry of the magnetic field profile with respect to the *z*=0 plane (Neumann condition) and the requirement of a mean circular induction B_p across the sample thickness, respectively. This problem is non linear, because $\underline{\mu}$ depends on $|\underline{H}|$. We thus discretize Eq. (5) versus *z* by the Finite Elements Method and we apply the Fixed Point (FP) iterative technique [5] to solve the non linearity. Its solution provides the $\underline{H}(z)$ profile, by which we can compute, via the constitutive equation, the classical loss $W_{class}^{(ROT,\,FP)}$ and obtain the hysteresis loss component $W_{hyst}^{(ROT)}$. The classical component is evaluated by integration on the lamination thickness of the square of the current density modulus derived from the numerical computation of the curl of the ***H*** field. The hysteresis loss is obtained by summing the areas of the local hysteresis cycles. Since the induction profile through the sample cross-section evolves with *f*, the same holds for $W_{hyst}^{(ROT)}$, as shown in Fig. 5. This behavior replicates to some extent the skin effect related increase of the hysteresis loss with *f* observed under alternating fields [5, 7], but for the decrease of $W_{hyst}^{(ROT)}$ at the highest J_p values. Such a decrease is consistent with the experimental dependence of $W_{hyst}^{(ROT)}$ on J_p. After having attained a maximum value, it tends to zero on approaching the saturation, following the disappearance of the domain walls. If we define the quantity $W^{(ROT,FP)} = W_{hyst}^{(ROT)} + W_{class}^{(ROT,\,FP)}$, the sum of the so-calculated hysteresis and classical losses, we find that it accounts for most of the measured loss $W_{exp}^{(ROT)}$ beyond f_{thr}, while the conventional loss separation holds below this threshold. Comparison of $W_{exp}^{(ROT)}$ with $W^{(ROT,FP)}$ is provided in Fig. 6 at f = 1 kHz and f = 100 Hz. In both cases the excess loss, though crucial to the identification of the threshold frequency f_{thr} via Eq. (1), turns out to be a few percent of the total loss only. It is observed how $W_{class}^{(ROT)}$, calculated with Eq. (1), overestimates the

measured loss at f = 1 kHz and low inductions, while falling short of $W_{class}^{(ROT,\ FP)}$ at high inductions, consistent with the results reported in Fig. 2.

We might inquire about a possible approximate expression for the classical rotational loss with skin effect where, as often done with the alternating regime [3, 21], a linear material is considered. With constant complex permeability $\underline{\mu}$, uniform across the lamination depth and depending only on the mean value B_p, we obtain a linear diffusion equation, which can be analytically solved. If the correspondingly calculated classical loss is $W_{class}^{(ROT,LIN)}$, a ratio $F_{class}^{(LIN)} = W_{class}^{(ROT,LIN)}/W_{class}^{(ROT)}$ is obtained through the equation

$$F_{class}^{(LIN)}(d/\delta) = 3\frac{(\sinh a_+ / a_+ - \sinh a_- / a_-)}{\cosh a_+ - \cos a_-} \tag{9}$$

where $\delta = 1/(\pi|\underline{\mu}|\sigma f)^{1/2}$ is the skin depth and $a_\pm = (1 \pm \varepsilon)\, d/\delta$, with $\varepsilon = \tan(0.5\cdot\arg(\underline{\mu}))$, is a dimensionless quantity. It is interesting to parallel the ratio $F_{class}^{(LIN)}$ with the one concerning the previous numerical solution for the classical loss $F_{class}^{(FP)} = W_{class}^{(ROT,FP)}/W_{class}^{(ROT)}$. These ratios are shown in Fig. 7 as a function of d/δ, with the frequency ranging between DC and 1 kHz, for different values of J_p. The linear model, always providing a ratio $F_{class}^{(LIN)} < 1$, cannot account for the effect of saturation on the lamination edges, a feature that can properly dealt with only by $W_{class}^{(ROT,\ FP)}$. Remarkably, at high inductions, where $F_{class}^{(FP)} \geq 1$ (but relatively close to 1, as shown in Fig. 7), assuming $F_{class} = 1$ (i.e. neglecting the skin effect) provides a better approximation of the experiments than the linear model.

4. Conclusions

Magnetic losses have been measured under circular induction in 0.640 mm tick low-carbon steel laminations up to frequencies of 1 kHz and peak polarization level J_p = 1.7 T. Relevant skin effect takes place, depending on the J_p value, starting from a few ten Hz, as uniquely revealed by the loss decomposition procedure, performed according to the statistical theory of losses. It is demonstrated that the classical loss component, always dominant beyond the threshold frequency for the skin effect, can be accurately computed exploiting a simplified magnetic constitutive law of the material under rotational field. It is also shown that the extreme simplification of assuming a fully linear approximation for the diffusion equation can provide at low induction levels better results than the well known formula of the classical loss without skin effect. On the contrary, at higher induction levels, the classical expression (neglecting skin effect) can provide a better approximation.

References

[1] K.M. Rahman and S.E. Sculz, Design of high-efficiency and high-torque-density switched reluctance motor for vehicle propulsion, *IEEE Trans. Ind. Appl.*, **38** (2002), 1500-1507.

[2] S. Niu, . Ho, W. Fu, and J. Zhu, Eddy current reduction in High-Speed Machines and Eddy Current Loss Analysis With Multislice Time-Stepping Finite-Element Method, *IEEE Trans. Magn.*, **48** (2012), 1007-1010.

[3] G. Bertotti, *Hysteresis in Magnetism*, Academic Press, New York, 1998, Chap. 12.

[4] E. Barbisio, F. Fiorillo, and C. Ragusa, Predicting Loss in Magnetic Steels Under Arbitrary Induction Waveform and With Minor Hysteresis Loops, *IEEE Trans. Magn.*, **40** (2004), 1810-1819.

[5] C. Appino, G. Bertotti, O. Bottauscio, F. Fiorillo, P. Tiberto, D. Binesti, J.P. Ducreux, M. Chiampi, and M. Repetto, Power losses in thick steel laminations with hysteresis, *J. Appl. Phys.* **79** (1996), 4575-4577.

[6] V. Basso, G. Bertotti, O. Bottauscio, F. Fiorillo, M. Pasquale, M. Chiampi, and M. Repetto, Power losses in magnetic laminations with hysteresis: finite element modeling and experimental validation, *J. Appl. Phys.* **81** (1997), 5606-5608.

[7] S. E. Zirka, Y.I. Moroz, P.Marketos, and A.J. Moses, Evolution of power loss components with induction level and frequency, *J. Magn. Magn. Mater*. **320** (2008), e1039-e1043.

[8] C. Beatrice, C. Appino, O. de la Barrière, F. Fiorillo, and C. Ragusa, Broadband magnetic losses in Fe-Si and Fe-Co laminations, *IEEE Trans. Magn.*, **50** (2014), 6300504.

[9] C. Appino, C. Ragusa, and F. Fiorillo, Can rotational magnetization be theoretically assessed?, *Int. J. Appl. Electromagn. Mech.*, **44** (2014), 355-370.

[10] Y. Li, J. G. Zhu, Q. Yang, Z. W. Lin, Y. Guo, and C. Zhang, Study on rotational hysteresis and core loss under three dimensional magnetization, *IEEE Trans. Magn.*, **47** (2011), 3520-3523.

[11] O. de la Barrière, C. Appino, F. Fiorillo, C. Ragusa, M. Lecrivain, L. Rocchino, H. Ben Ahmed, M. Gabsi, F. Mazaleyrat, and M. LoBue, Extended frequency analysis of magnetic losses under rotating induction in soft magnetic composites, *J. Appl. Phys.*, **111** (2012), 07E325.

[12] C. Appino, O. de la Barrière, C. Beatrice, F. Fiorillo, and C. Ragusa, Rotational magnetic losses in nonoriented Fe–Si and Fe–Co laminations up to the kilohertz range, *IEEE Trans. Magn.*, **50** (2014), to appear.

[13] C. Ragusa and F. Fiorillo, A three-phase single sheet tester with digital control of flux loci based on the contraction mapping principle, *J. Magn. Magn. Mater*., vol. 304, no. 2 (2006), pp. e568-e570.

[14] Y. Guo, J. Zhu, J. Zhong, H. Lu, and J. Jin, Measurement and modeling of rotational core losses of soft magnetic materials used in electrical machines: a review, *IEEE Trans. Magn.*, **44** (2008), 279-291.

[15] E. Cardelli, A. Faba, and F. Tissi, *Int. J. Appl. Electromagn. Mech.*, **44** (2014), 331-338.

[16] C. Appino, F. Fiorillo, and C. Ragusa, One-dimensional/two-dimensional loss measurements up to high inductions, *J. Appl. Phys.* **105** (2009), 07E718.

[17] S. Steentjes, S.E. Zirka, Y.E. Moroz, E.Y. Moroz, and K. Hameyer, Dynamic magnetization model of nonoriented steel sheets, *IEEE Trans. Magn.*, **50** (2014), 7300204.

[18] A.J. Bergqvist, A simple vector generalization of the Jiles-Atherton model of hysteresis, *IEEE Trans Magn.* **32** (1996), 4213–4215.

[19] I. D. Mayergoyz, *Mathematical Models of Hysteresis and Their Applications*, Academic Press-Elsevier, 2003.

[20] S.E. Zirka, Y.I. Moroz, P. Marketos, and A.J. Moses, Viscosity-based magnetodynamic model of soft magnetic materials, *IEEE Trans. Magn.*, **42** (2006), 2121-2132.

[21] K. Simonyi, A. Sekey, *Foundations of Electrical Engineering: Fields-networks-waves*, Macmillan, 1963.

Figure captions

Fig. 1 – Rotational energy loss vs. J_p measured in a 0.640 mm thick low-carbon steel sheet in the range of frequencies 2 Hz - 1 kHz.

Fig. 2 – a) The experimental values of $W_{diff}^{(ROT)}(f) = W^{(ROT)}(f) - W_{class}^{(ROT)}(f)$ (symbols), with $W_{class}^{(ROT)}(f)$ given by Eq. (1), diverge from the standard $f^{1/2}$ law beyond a threshold frequency, signaling the surge of the skin effect. b) At the same frequency the correspondingly calculated number of active magnetic objects $n(H_{exc})$ versus H_{exc} behavior suffers a sharp turnabout.

Fig. 3 – The experimental quasi-static $\boldsymbol{H}$-locus is assimilated to a circular locus of same area, belonging to the equivalent perfectly isotropic material.

Fig. 4 – Quasi-static rotational permeability $\mu = B_p / H_0$ and related angular delay θ_{hyst} of B_p (see Fig. 3).

Fig. 5 – Skin effect dependent evolution of the hysteresis energy loss with frequency. Decrease of $W_{hyst}^{(ROT)}$ with f is observed at highest J_p values, because the material attains saturation on the outer sheet layers.

Fig. 6 – Measured rotational loss $W_{exp}^{(ROT)}$ versus polarization J_p at f = 1 kHz and f = 100 Hz and its comparison with the quantity $W^{(ROT,FP)} = W_{hyst}^{(ROT)} + W_{class}^{(ROT,\ FP)}$ (solid line) calculated via the electromagnetic diffusion equation and its solution by the Fixed Point technique. The dash-dotted lined shows the behavior of $W_{class}^{(ROT)}$ calculated with the standard Eq. (1).

Fig. 7 - Ratios $F_{class}^{(FP)} = W_{class}^{(ROT,FP)}/W_{class}^{(ROT)}$ and $F_{class}^{(LIN)} = W_{class}^{(ROT,LIN)}/W_{class}^{(ROT)}$ (with $W_{class}^{(ROT)}$ given by Eq. (1)) calculated by the numerical method with Fixed Point iteration and the linear method. d / δ is the ratio between the sheet thickness and the skin depth.

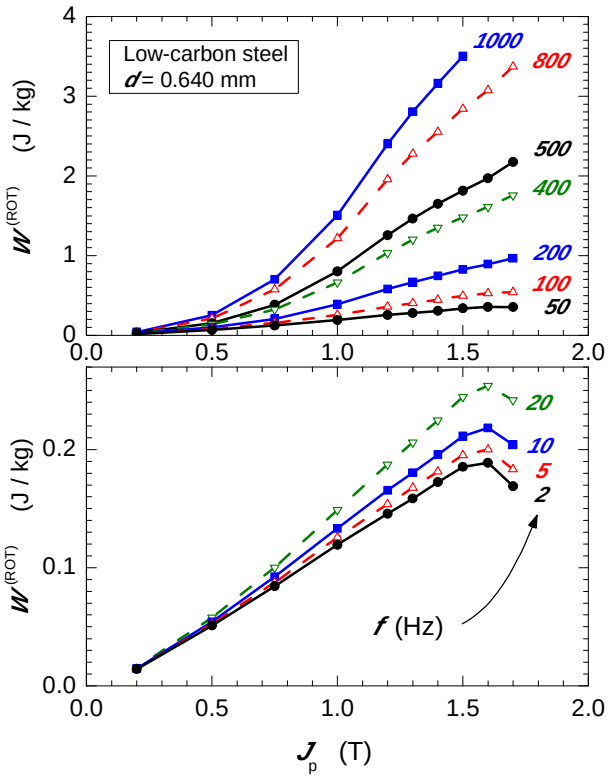

Fig. 1 – Rotational energy loss versus circular polarization J_p measured in a 0.640 mm thick low-carbon steel sheet in the frequency range 2 Hz - 1 kHz.

255

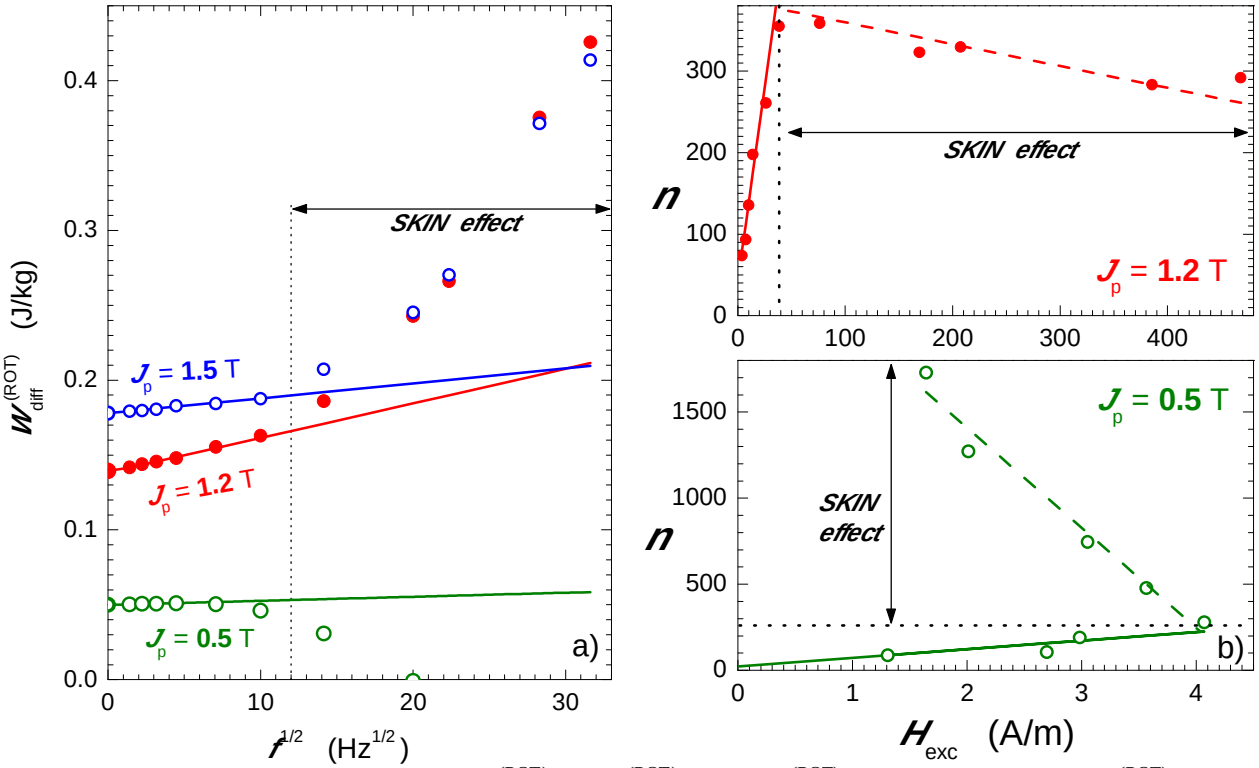

Fig. 2 – a) The experimental values of $W_{diff}^{(ROT)}(f) = W^{(ROT)}(f) - W_{class}^{(ROT)}(f)$ (symbols), with $W_{class}^{(ROT)}(f)$ given by Eq. (1), diverge from the standard $f^{1/2}$ law beyond a threshold frequency, signaling the surge of the skin effect. b) At the same frequency the correspondingly calculated number of active magnetic objects $n(H_{exc})$ versus H_{exc} behavior suffers a sharp turnabout.

256

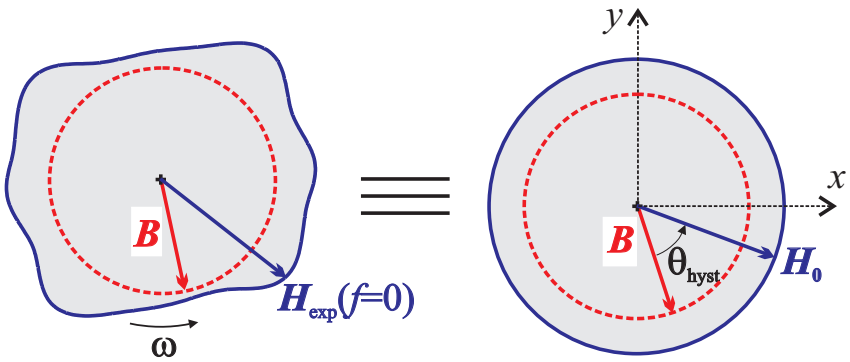

Fig. 3 – The experimental quasi-static ***H***-locus is assimilated to a circular locus of same area, belonging to the equivalent perfectly isotropic material.

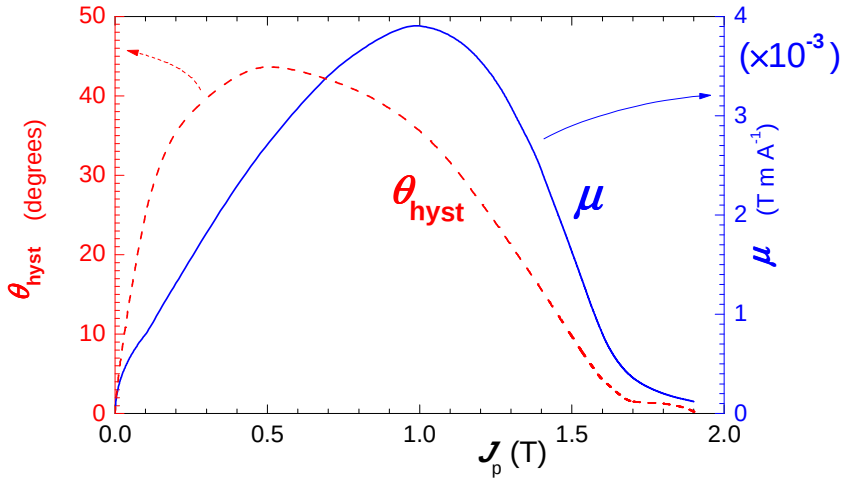

Fig. 4 – Quasi-static rotational permeability $\mu = B_p / H_0$ and related angular delay θ_{hyst} (see Fig. 3).

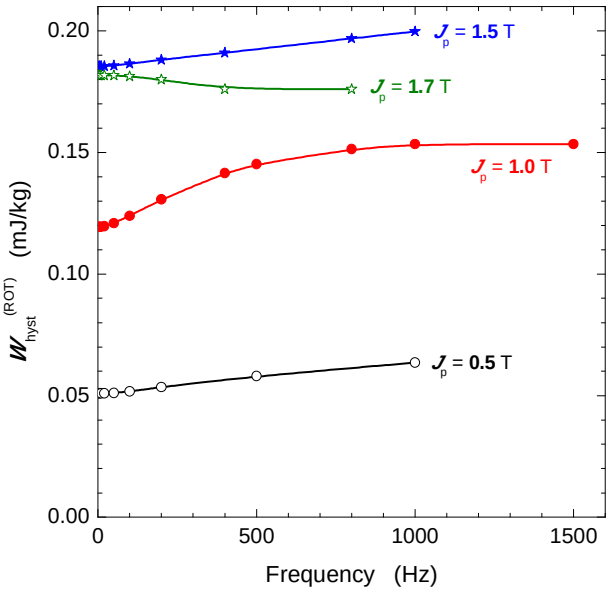

Fig. 5 – Skin effect dependent evolution of the hysteresis energy loss with frequency. Decrease of $W_{hyst}^{(ROT)}$ with f is observed at highest J_p values, because the material attains saturation in the outer sheet layers.

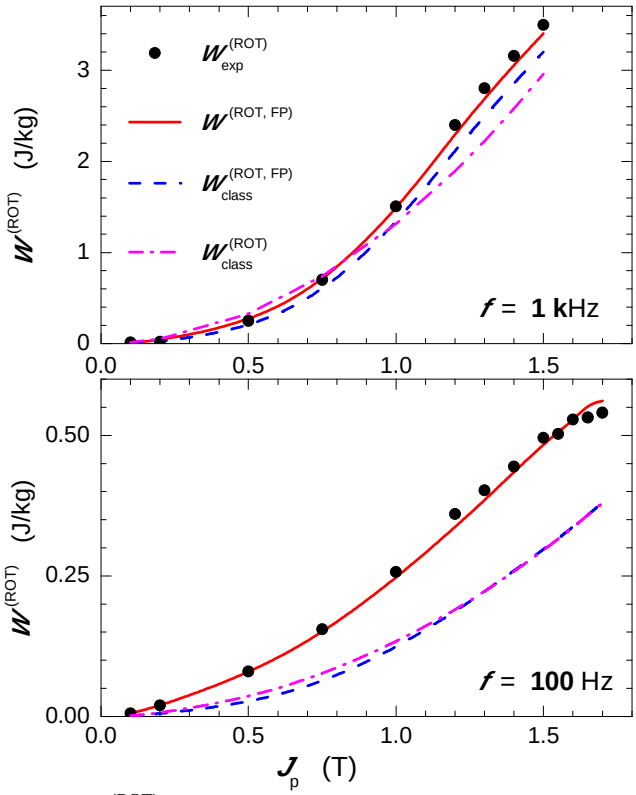

Fig. 6 – Measured rotational loss $W_{exp}^{(ROT)}$ versus polarization J_p at f = 1 kHz and f = 100 Hz and its comparison with the quantity $W^{(ROT,FP)} = W_{hyst}^{(ROT)} + W_{class}^{(ROT,\ FP)}$ (solid line) calculated via the electromagnetic diffusion equation and its solution by the Fixed Point technique. The dash-dotted lined shows the behavior of $W_{class}^{(ROT)}$ calculated with the standard Eq. (1).

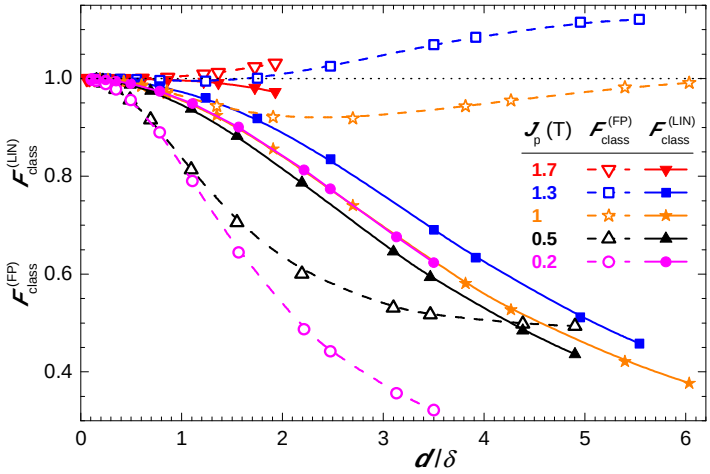

Fig. 7 - Ratios $F_{class}^{(FP)} = W_{class}^{(ROT,FP)}/W_{class}^{(ROT)}$ and $F_{class}^{(LIN)} = W_{class}^{(ROT,LIN)}/W_{class}^{(ROT)}$ (with $W_{class}^{(ROT)}$ given by Eq. (1)) calculated by the numerical method with Fixed Point iteration and the linear method. d / δ is the ratio between the sheet thickness and the skin dept